Targeting Autophagy Peptidase ATG4B With A Novel Natural Product Inhibitor Azalomycin F4a For Advanced Gastric Cancer

Lin Zhong
Sun Yat-Sen University 2nd Affiliated Hospital: Sun Yat-Sen Memorial Hospital
Bin Yang
Sun Yat-Sen University 2nd Affiliated Hospital: Sun Yat-Sen Memorial Hospital
Zhenhua zhang
Sun Yat-Sen University
Xiaojuan Wang
Tsinghua University Affiliated Beijing Tsinghua Changgung Hospital: Beijing Tsinghua Changgung Hospital
Yinfeng Guo
Sun Yat-Sen University
Weifeng Huang
Sun Yat-Sen University
Qianqian Wang
Sun Yat-Sen University
Guodi Cai
Sun Yat-Sen University
Fan Xia
Sun Yat-Sen University
Shengning Zhou
Sun Yat-Sen University 2nd Affiliated Hospital: Sun Yat-Sen Memorial Hospital
Shuai Ma
Sun Yat-Sen University 2nd Affiliated Hospital: Sun Yat-Sen Memorial Hospital
Yichu Nie
Sun Yat-Sen University
Jinping Lei
Sun Yat-Sen University
Min Li
Sun Yat-Sen University
Peiqing Liu
Sun Yat-Sen University

Wenbin Deng
Sun Yat-Sen University
Yonghong Liu
South China Sea Institute of Oceanology Chinese Academy of Sciences
Junfeng Wang
South China Sea Institute of Oceanology Chinese Academy of Sciences
Fanghai Han
Sun Yat-Sen University 2nd Affiliated Hospital: Sun Yat-Sen Memorial Hospital
Junjian Wang (wangjj87@mail.sysu.edu.cn)
Sun Yat-Sen University https://orcid.org/0000-0002-5328-2908

Research Article

Keywords: ATG4B, Azalomycin F4a, Gastric cancer, autophagy, metastasis

Posted Date: July 1st, 2021

DOI: https://doi.org/10.21203/rs.3.rs-663447/v1

Version of Record: A version of this preprint was published at Cell Death & Disease on February 1st, 2022. See the published version at https://doi.org/10.1038/s41419-022-04608-z.

Abstract

Background: Advanced gastric cancer (GCa) remains highly lethal due to the lack of effective therapies. Identifying promising therapeutic targets and developing effective treatment against GCa are urgently needed. Here, we investigated whether Autophagy-related gene 4B (ATG4B) could be a potential therapeutic target against GCa and identified marine natural product Azalomycin F4a (Am-F4a) as a potent ATG4B inhibitor and a potential anticancer agent.

Methods: The expression of ATG4B in clinical GCa tumor specimens were examined by immunoblotting and interrogation of public databases. The association between ATG4B expression and patient's survival was assessed. FRET, surface plasmon resonance, transmission electron microscopy analysis, enzyme activity assay and compute docking were used to assess the binding and inhibition of ATG4B by Am-F4a. RNA interference, inhibitors, CCK-8 cell viability assay, colony formation, apoptosis assay, wound-healing, transwell invasion assay, western blotting and Patient-derived organoids were used to assess the role of ATG4B in GCa cells. GCa cell-derived xenograft models, patient-derived xenografts and orthotopic metastasis xenografts were used to evaluate the anti-tumor growth and anti-metastasis effects of Am-F4a alone or in combination with 5-FU *in vivo*.

Results: ATG4B was highly upregulated in GCa tumors. Its high expression was associated with patient's poor prognosis. knockdown of ATG4B significantly inhibited GCa cell survival and tumor growth. Am-F4a was identified as a novel and potent ATG4B inhibitor. Am-F4a effectively inhibited GCa cell autophagy and growth via targeting ATG4B both *in vitro* and *in vivo*. Besides, both pharmacological inhibition and knockdown of ATG4B significantly suppressed GCa cell migration and invasion. Am-F4a potently blocked the metastasis of primary GCa tumors and effectively sensitized tumors to chemotherapy.

Conclusion: These findings indicate that ATG4B is a potential novel therapeutic target against GCa and that the natural product Am-F4a is a novel ATG4B inhibitor that can be further developed for treatment of GCa.

Background

Gastric cancer (GCa) is an aggressive cancer and the fourth leading cause of cancer-related death worldwide(1). It is characterized by rapid cancer progression and widespread metastasis. Approximately 60% of GC patients initially diagnosed with occurs local or distant metastasis(2), which accounts for about 90% cancer-associated death(3, 4)Over the past two decades, the development of surgical operation and neoadjuvant chemotherapy (NACT) have significantly improved the 5-year overall survival rate of patients with localized GCa (> 60%), whereas the 5-year overall survival rates of GCa patients with local and distant metastasis are approximately 30% and 5%, respectively(5–7). So far, chemotherapy remains the backbone of advanced GCa treatment, although it only modestly improves patient's survival(8). Recently, targeted therapies in GCa have made promising progress. Trastuzumab, a HER2 monoclonal antibody, was approved for advanced HER2-positive GCa treatment and successfully

improved patient's survival(7, 9–11). In addition, antibodies against VEGFR-2 (ramucirumab) and PD-1 (nivolumab or pembrolizumab), as second line and third line treatments, also improved overall survival of patients with advanced GCa(7, 12). However, options of targeted therapy for GCa are still limited and they only benefit a small fraction of patients, therefore, identifying novel anti-tumor targets and developing effective drugs for advanced GCa is urgently needed.

Autophagy-related gene 4 (ATG4) is a cysteine protease required for autophagosome formation and consists of 4 homologues - ATG4A, ATG4B, ATG4C and ATG4D(13). ATG4B shows high proteolytic activity on autophagy marker Atg8 orthologs (GATE-16, GABARAP, LC3, and Apg8L)(14, 15), while ATG4A only works on GABARAP subfamily proteins and ATG4C/D are almost inactive(16, 17). In ATG4B knockout mice, ATG4B depleted tissues exhibit notable defects in LC3-II conversion, autophagic flux and autophagosome formation(18, 19). Dysregulated autophagy tightly correlates with tumorigenesis and cancer progression. Accumulating studies suggest that ATG4B play oncogenic roles in a number of cancers, such as colorectal cancer and glioblastoma(GBM)(20). ATG4B is overexpressed in tumor cells of colorectal patients. Pharmacological and genetic inhibition of ATG4B inhibited colorectal cancer cell proliferation and xenograft tumor growth(14). In GBM cells, ATG4B inhibition significantly suppressed cellular autophagic activity and tumorigenicity, as well as enhanced the anti-GBM efficacy of radiotherapy(21). In addition, ATG4B overexpression conferred cancer drug resistance while its inhibition markedly sensitized tumors to chemotherapy in lung cancer(22), colon cancer(23) and chronic myeloid leukemia(24). These studies indicate that ATG4B is a potential anticancer target. However, the function of ATG4B in GCa is unclear.

Although several ATG4B inhibitors (S130, NSC185058, Tioconazole, et al) have been identified(14, 25, 26),but their activity and selectivity is limited. Development of novel and potent ATG4B inhibitors with different scaffolds are still needed to explore the therapeutic potential of targeting ATG4B in cancer. Natural products exhibit high diversity in chemical structures and are one major source of drug development(27). More than 40% of the approved anti-cancer drugs, including first line chemotherapy drug paclitaxel, etoposide and irinotecan, were either natural products or derived from natural products(27, 28). Recently, drug development from marine natural products gained much attention. There are remarkably high hit rates from marine source, due to their unique and diverse molecular structures(29). Several marine-derived compounds include Adcetris®(30), Halaven®(31), Yondelis®(32), and Cytosar-u®(33) have already been approved for cancer therapy. In addition, new technologies have markedly accelerated the discovery of novel marine natural products and drug candidates.

In this study, we found that high ATG4B expression correlated with poor survival of patients with gastric cancer and was essential for tumor growth. We also discovered a novel ATG4B inhibitor Am-F4a from a marine natural product library. The compound could effectively suppress GCa cell growth both *in vitro* and *in vivo*. Furthermore, ATG4B inhibition significantly blocked the progression of GCa metastasis. Therefore, our results suggest that targeting ATG4B with the novel inhibitor Am-F4a might be a new approach to treat advanced GCa.

Methods And Materials

Cell culture and reagents

The AGS, MKN45,HGC27,SNU1,KATO and 293T cells were obtained from the American Type Culture Collection (ATCC). Human gastric cancer cell lines MGC803, were purchased from China Academia Sinica (Shanghai, PR China). The gastric cancer MGC803, AGS, MKN45, HGC27, SNU1, KATO cells were cultured in RPMI-1640 medium and HEK293T embryonic kidney cells were cultured in DMEM medium, supplemented with 10% fetal bovine serum and 1% penicillin/streptomycin in a humidified incubator at 37°C with 5% CO2. Antibodies against the following proteins were used with source and dilution ratios indicated: ATG4B (Cell signaling; #13507; 1:1000 and Proteintech; # Cat No. 15131-1-AP ; 1:1000); P62(Sigma,#P0067,1:1000), LC3(Sigma;# ABC929,1:1000), Snail, (CST,#4719,1:1000), N-cadherin(CST,#4061,1:1000), C-caspase7(CST,#12827,1:1000), PARP-1 (CST,#9542,1:1000), GAPDH(CST,#2118,1:1000). AzalomycinF4a was isolated from *Streptomyces solisilvae* HNM30702 and verified by the NMR and HRESIMS data(34). Rapamycin (MCE, #HY-10219), BafilomycinA1MCE,# HY-100558 Tioconazole (MCE,#HY-1303191 CS-2360), Acridine Orange(Sigma,#MKCD9806), Lyso-Tracker Red(Pythonbio,#L12492), FMK9a(MCE,HY-100522).

Analysis of ATG4B expression and Kaplan-Meier survival curve in clinical tumors

Publicly available gastric cancer expression datasets GSE13911 and GSE19826 were downloaded from GEO at http://www.ncbi.nlm.nih.gov/geo/. The datasets contain gene expression profiles of normal and gastric cancer tumor samples. The expression of ATG4B in different groups was analyzed as described previously. For Kaplan-Meier survival curve analysis, patients with GCa tumors were stratified by the ATG4B transcript levels, the overall survival and relapse free survival of patients was analyzed using an online survival analysis tool (http://kmplot.com/), statistical significance were assessed by the log-rank test.

Western blotting, siRNA transfection and shRNA lentivirus transduction

Western blotting was performed with the indicated primary antibodies as our previous reports(35). For siRNA transfection, siRNAs were obtained from Sangon Biotech(shanghai)Co.,Ltd. The siRNA sequences for ATG4B are as followings: siATG4B#1, GAAAGAUUCGACUCAGAATT; siATG4B#2, GGUGUGGACAGAUGAUCUUUGTT; siControl, CAGUCGCGUUUGCGACUGG. For shRNA assay, the ATG4B shRNA sequence was as follows: ATG4B: 5'-TGATGTGGCATCTAGACTTTG-3'; it was purchased from Sangon Biotechshanghai Co.,Ltd and cloned into a PLKO.1 lentivirus vector. ATG4B and control shRNA Lentiviral particles were produced in 293T cells after co-transfected with the lentivirus vectors, packaging plasmid psPAX2 and envelope plasmid pMD2.G. siRNA transfections and shRNA lentivirus transduction were performed as described previously.

Cell growth and colony formation

For cell growth, GCa cells were seeded in 6 well plates at 1× 10^6 per well in triplicate. After indicated48 hours of drug treatment, total viable cell numbers were counted by a cell counter. In addition, the cell viability was also determined by CCK-8 assay (kit. 40203ES60*, Yeasen, China). Briefly, cells were seeded in 96-well plates at 800 cells per well, after 12 hours, different dose compounds were added to cell culture medium and cells were cultured for another 96 hours. Cell viability were measured by a CCK-8 kit according to the manufacturer's instruction. For colony formation, GCa cells were seeded in 6-well plates at 800 per well and cultured for 7–12 days, cell culture medium containing indicated compounds were replaced every 3 days. Cells were then fixed in 4% paraformaldehyde for 15 min, and then washed with PBS three times. Cell colonies were stained with crystal violet for 30 min and washed with PBS six times. Colonies consisted of more than 50 cells were counted and graphed.

Migration and invasion assays

The migration of GCa cells were determined using would healing assay. Briefly, when cells in 6-well plates were ~ 100% confluent, cell monolayer were scratched using pipette tips. Cell culture medium were replaced and drugs were added. After indicated time, the images of the wound were photographed by a microscope and wound closure rates were calculated. Cell invasion assay were performed using transwell chamber (Costar, USA). Upper insert of chamber were plated with 100 μL matrigel per well and kept in 37°C incubator for 4 hours. 300 μL serum-free RPMI-1640 medium containing GC cells (1–2 × 10^5) were added into the upper insert, 500μl RPMI-1640 containing 5% FBS was added to the bottom chamber. After cells were treated with indicated drugs for 24 hours, invading cells were fixed with 4% paraformaldehyde and stained with crystal violet staining dilution. Cells were counted in five randomly microscope field each well and experiments were conducted in triplicate.

Molecular docking

The crystal structure of human ATG4B (PDB code: 2CY7.pdb) downloaded from Protein Data Bank (http://www.pdb.org) was used for the molecular docking. The molecular docking was performed by Schrodinger program following our previous study (36). The ligand and protein structure preparation, including water deletion, protonation-state adjustment, and hydrogen atoms and disulfide bonds adding were performed by Maestro (version 11.6.013, Schrödinger, LLC, New York, NY, 2018). The Glide docking program in Maestro 11.6.013 was used for docking studies. The designed molecule Am-F4a was docked into ATG4B using Glide SP mode, the grid was defined using a 45 Å box centered on the CG atom of residue LEU11 of ATG4B. All other parameters were kept as default. The PyMOL software (DeLano Scientific, Palo Alto, CA, USA) was used to obtain the 3D structure of the docking model.

FRET assay and surface plasmon resonance (SPR) analysis

The inhibition of compounds on ATG4B activity was performed as our previous report(35). The percentage of inhibition was used to plot drug concentration-response curve and calculate IC50 values (Graphpad 8.0, GraphPad Software, La Jolla, CA, USA). The binding affinity of Am-F4a and Atg4b protein

was measured by SPR assay on a Biacore 8K instrument (GE Healthcare, Piscataway, NJ, USA). Briefly, purified ATG4B protein (200 μg/ml, pH 8.0) were immobilized (~ 10,000RU) on a Series S Sensor Chip (GE Healthcare, Piscataway, NJ, USA) according to a standard amine coupling procedure. running buffer for immobilization was PBS (Servicebio, G0002,pH7.2-7.4) containing 5% DMSO. After immobilization, compound Am-F4a serially diluted in running buffer was as stock solution. Seven concentrations of Am-F4a (20, 10, 5, 2.5, 1.25, 0.625, 0 μM) were simultaneously injected at a flow rate of 65 μl/min for 60 sec of association phase at 25℃. Biacore 8K manager software was used to calculate equilibrium dissociation constant (Kd).

GFP-LC3 translocation and lysosomal function analysis

MGC803 cells were transfected with the plasmid encoding mRFP-eGFP-LC3 as described previously (14). After 24 hours, MGC803 cells expressing mRFP-eGFP-LC3 were treated with compounds at the indicated concentrations. For lysosomal function analysis, cells were treated with Am-F4a (10 μM),Rap (1 μM) ,Baf(0.5μM)or Chloroquine（CQ,40μM）for 4 h, followed by staining with Lyso-Tracker Red (LTR, 50 ng/ml) or Acridine Orange (AO, 0.5μg/ml) for 30 min. Fluorescence images of live cells were taken by confocal microscopy (Olympus Corporation, Japan).

Transmission electron microscopy (TEM)

MGC803 cells in 6-well plates were fixed in 2.5% glutaraldehyde for 2 hours, and then dehydrated in a graded ethanol series and embedded. Ultrathin sections were mounted and post-stained with 2% uranyl acetate followed by 0.3% lead citrate. Sections were imaged using a transmission electron microscope G2 20 Twin (FEI, USA).

Patients and specimens

The gastric cancer and normal tissues of patients were obtained from Sun Yat-sen Memorial Hospital of Sun Yat-sen University, Guangzhou, China. all the specimens were confirmed by pathological examination. Informed consent was obtained from all patients. All clinical studies were approved by the Clinical Research Ethics Committee of Sun Yat-sen University, and were performed in accordance with approved guidelines (Helsinki Declaration of 2013).

Mouse models and treatments

All procedures were conducted in accordance with the “Guiding Principles in the Care and Use of Animals” (China) and were approved by the Animal Ethics Committee at Sun Yat-sen University. Four-week-old male NOD/SCID mice were purchased from Gempharmatech Inc (China). BALB/c nu/nu mice were purchased from Experimental Animal Center of Sun Yat- Sen University. Approximately 5×10^6 MGC803 cells were suspended in total of 100 μL PBS and Matrigel (1:1) and implanted subcutaneously into the dorsal flank on both sides of the BALB/c nu/nu mice. When the tumor volume was approximately 50 mm^3, the mice were randomized and treated intraperitoneally (i.p.) as indicated for five times per week. Tumor growth was monitored by calipers and volume was calculated using the equation: $\pi/6$ (length × $width^2$). Body weight during the course of the study was also monitored. At the end of the

studies, mice were sacrificed and tumors were dissected and weighed. To assess the effect of shRNA mediated silencing of ATG4B on GCa xenograft tumor growth. 5×10^6 MGC803 cells infected with lentivirus shControl or shATG4B were implanted into the dorsal flank of mice as above. Tumor volume and mice body weight was monitored. For the patient-derived xenograft, tumor sample was from patient with GCa adenocarcinoma. Characteristics of this patient are as followings: male, 42 years, Asian, primary GCa tumor, AJCC IB/grade 3, surgical sample. The GCa tumor tissues were divided into ~ 2 mm^3 micro tissues and were engrafted subcutaneously into the mice dorsal flank. The effect of drugs on the PDX tumor growth was monitored as above description. For orthotopic mice xenografts, four-week-old male NOD/SCID mice abdomen was incised, $1x10^7$ cells MKN-45 cells stable expressing luciferase were injected into the subserosal layer of the stomach with a needle. Tumors growth in the stomach wall and metastases to the peritoneal cavity or other organs were monitored by Bioluminescence imaging. Mice body weight was also monitored. At the end of the studies, mice were sacrificed and tumors were dissected and weighed.

Patient-derived organoids (PDO) culture

Organoids were cultured from fresh dissected tumors of PDX xenografts when the tumor size was ~ 500 mm^3. Briefly, dissected tumors were finely minced and transferred to a 50-ml conical tube, including a digestion mix consisting of serum-free DMEM/F-12 medium and 1 mg/ml collagenase IV (Sigma), and incubated for 1 h at 37°C. Isolated organoids were mixed with 50 µl of Matrigel and seeded in 96-well plates. The culture medium contains phenol red-free DMEM/F-12 with primocin (50 mg/ml), B27 supplement (1×), FGF 7 (5 ng/ml), R-Spondin 3 (250 ng/ml),penicillin/streptomycin/glutamine (100 mg/ml), Y-27632 (5 mM),Hepes (10 mM), A83- 01 (500 nM), neuregulin 1 (5 nM), FGF 10 (20 ng/ml), EGF (100ng/ml), SB202190 (500 nM), N-acetylcysteine (1.25 mM) and nicotinamide (5 mM). One milliliter of supplemented culture medium was added per well, and organoids were maintained in a 37°C humidified atmosphere under 5% CO2. After one week, PDX-derived organoids were treated with DMSO or Am-F4a for another 3 days, representative images were taken under a fluorescence microscope, and cell viability in organoids was measured with Cell Titer-Glo.

Statistics

Results were expressed as mean values ± S.E.M or mean values ± SD from at least 3 independent experiments. Statistics analysis were assessed using the Student's 2-tailed t test. *$P < 0.05$ was considered as being significant.

Results

ATG4B is highly overexpressed in GCa clinical tumors and required for GCa cell growth

Our previous studies revealed that ATG4B is a potential therapeutic target in colon cancer(14). This promoted us to examine whether ATG4B exerted critical functions in other cancer types. Analysis of GEO datasets showed that the mRNA level of ATG4B was significantly higher in gastric cancer tumors than in

normal tissues (Fig. 1a). Consistently, ATG4B protein was easily detectable in GCa cell lines(supplementary Fig. 1a)by immunoblotting analysis and its level was markedly enhanced in representative GCa tumors compared with paired primary tissues (Fig. 1b and supplementary Fig. 1b). Paired t test performed on the results of immunoblotting analysis revealed that ATG4B was overexpressed in over 50% of the tumors (Fig. 1c). Kaplan–Meier survival analysis demonstrated that high ATG4B was strongly correlated with poor overall survival outcome of patients with GCa (Fig. 1d). These data indicate that ATG4B could be a potential GCa prognostic biomarker.

We next examined the function of ATG4B in gastric cancer cell lines. Silencing ATG4B with two specific siRNA demonstrated that ATG4B knockdown significantly inhibited cell proliferation and induced apoptosis in gastric cancer lines MGC803 and AGS (Fig. 1e,1f). Consistently, ATG4B silencing also markedly decreased GCa cell's colony formation ability (Fig. 1g). Encouraged by our in vitro results, we further assessed whether ATG4B contributes to GCa tumorigenesis in vivo. Employing GCa cell-based xenograft models, we found that ATG4B knockdown effectively blocked tumorigenesis and growth (Fig. 1h) At 40 days after the implantation of MGC803 cells, most of the mice with shATG4B-treated cells did not develop measurable tumors while the tumor volume in shControl group reached 600 mm^3 in average (Fig. 1h,1i,1j). These results suggested that ATG4B be a critical gene in GCa tumorigenesis and growth.

Identification of Am-F4a as a novel ATG4B inhibitor

Several ATG4B inhibitors have been identified and reported in literature, (13) however, their efficacy and structural diversity are rather limited. To further explore the pharmacological functions of ATG4B in GCa, we firstly employed an in vitro FRET assay based on ATG4B catalytic activity to screen a natural product library,which contains more than 400 marine natural compounds. The 36-membered macrocyclic antitumor azalomycin F4a (Am-F4a) is the main products of Streptomyces solisilvae HNM30702, which possesses one characteristic guanidino group rarely discovered in nature (Fig. 2a). As shown in Fig. 2b and 2c, Am-F4a effectively inhibited ATG4B activity with IC501.13×10^{-5}mol, in FRET assay. The gel-based assay which we previously developed(37)confirmed that Am-F4a strongly suppressed the proteolytic activity of ATG4B using FRET-GATE16 as substrate (Fig. 2b, 2c). Surface plasmon resonance (SPR) showed that Am-F4a could directly bind to ATG4B with a dissociation constant of 1.18×10^{-5}mol/L (Fig. 2d). Moreover, Am-F4a showed reasonable selectivity against ATG4A (Fig. 2e) with only 10% inhibitory activity at 20μg/ml. To understand the inhibitory mechanism of Am-F4a at molecular level, we performed molecular docking of Am-F4a with ATG4B protein structure. The Am-F4a was docked into a binding pocket that is composed of Thr10, Leu11, Phe13, Ala14, Glu15, Glu17, Pro260, Asn261, Ser262, Glu273, Tyr276, Asp278, His280, Cys306, Arg307, Met308, Ser309 and Glu312 (Fig. 2f, 2g) as reported in our previous works.(14, 37)As shown in Fig. 2d, Am-F4a binds to the protein through potential hydrogen bonds with residues Glu15, Asn261, Tyr276, Arg307, Ser309 and Glu312. Especially, the guanidine group of Am-F4a could form hydrogen bonding interactions with Asn261 which is part of the regulatory loop (residues Lys259, Pro260, Asn261 and Ser262) covering the entrance of catalytic site and going through

large conformational changes when LC3 interacts with ATG4B(37, 38). These results collectively confirm that Am-F4a is a potent ATG4B inhibitor.

Am-F4a suppresses autophagy flux and accumulates autolysosomes with more lipidated LC3

Given the crucial functions of ATG4B in autophagy, we examined whether its inhibitors affected autophagy process in GCa cells. LC3B-Ⅱ and P62 are validated indicators of autophagy activity of ATG4B(39, 40). Our immunoblotting results showed that Am-F4a caused significant accumulation of LC3B-Ⅱ and increased the protein level of P62 substantially, which suggested that Am-F4a treatment resulted in autophagosome accumulation in GCa cells (Fig. 3a). We next used a tandem mRFP-eGRP-LC3 construct to analyze the changes of autophagic flux as we previously reported(14). Briefly, an acidic lysosome environment leads to reduction of the pH-sensitive green fluorescence (GFP) and keeps red fluorescence (RFP), autophagosomes display both mRFP and GFP signals while lysosomes exhibit high mRFP signals and low GFP signals, which can be used to indicate the fusion step of autophagosomes with lysosomes. As expected, Rapamycin (Rap, an autophagy inducer) treatment resulted in greater red-only fluorescent puncta in the GCa cells, while Am-F4a- and Bafilomycin (Baf, an autophagy inhibitor) - treated cells showed high level of yellow puncta, from a mixture of GFP and RFP (Fig. 3b). The results suggested that Am-F4a might efficiently suppress autophagic flux. To examine whether the effect of Am-F4a on autophagy was caused by lysosome dysfunction, the pH of lysosome was measured with Lyso-Tracker Red (LTR) and acridine orange (AO).(14)Compared with control cells, there was no significant change in fluorescence in Am-F4a-treated cells, suggesting that Am-F4a did not cause the dysfunction of lysosome (Fig. 3c ,3d). Furthermore, we used transmission electron microscopy to analyze the effect of Am-F4a on cellular ultrastructural morphological changes. Images showed that Am-F4a-treated cells accumulated more autophagosomes compared to the control cells (Fig. 3e). Taken together, these data suggested that Am-F4a treatment result in the accumulation of autophagosomes and the suppression of autophagy flux in GCa cells.

Am-F4a inhibits GCa cell growth via inhibition of ATG4B and improve anti-GCa efficacy of 5-FU

The prominent inhibition of Am-F4a on ATG4B activity and autophagy promoted us to examine whether Am-F4a mediates cell fate in GCa. Indeed, our results showed that Am-F4a significantly inhibited the growth of GCa cell MGC803 and AGS (Fig. 4a). Consistently, the growth inhibition by another established ATG4B inhibitor tioconazole (TC) was also observed (Fig. 4a). In line with the inhibition of survival by ATG4B siRNA, treatment of MGC803 and AGS cells with Am-F4a or TC potently reduced cell colony formation and induced cell apoptosis, as compared to treatment with vehicle (Fig. 4b,4c). Because PDX-derived organoids can precisely imitate clinical tumors in response to therapeutics,we treated organoids with Am-F4a to investigate its therapeutic potential. We found Am-F4a can significantly inhibit the growth of organoids (Fig. 4d,4e). To provide further evidence that Am-F4a decreased the viability of GCa cell via inhibiting ATG4B activity, we demonstrated that the inhibitory effect of Am-F4a on GCa cell growth was obviously attenuated in ATG4B siRNA treated cells compared to control cells (Fig. 4f). Since accumulating studies showed that autophagy inhibitors might improve the effects of chemotherapy in various cancer types(41), we wondered whether ATG4B inhibitors have the same function in GCa. As shown in Fig. 4g, pharmacological inhibition of ATG4B by Am-F4a or TC significantly enhanced

antiproliferation of 5-FU treatment on GCa cells. Next, we performed clonogenic survival assay and found a highly synergistic inhibitory effects on the survival of GCa cells after they were treated by a combination of 5-FU and either Am-F4a or TC (Fig. 4h). These results collectively indicated that pharmacological inhibition of ATG4B with the novel inhibitor Am-F4a or TIC might effectively inhibit the viability of GCa cells via suppressing ATG4B activity and improve anti-GCa efficacy of 5-FU.

Pharmacological inhibition of ATG4B with Am-F4a inhibits GCa tumor growth and improves 5-FU treatment *in vivo*

To evaluate the therapeutic efficacy of Am-F4a against gastric cancer *in vivo*, we generated xenografts in immune-deficient nude mice from MGC803 cells. When the volume of tumors reached approximately 50 mm^3, the mice were randomized into four groups and treated with vehicle, Am-F4a (5mg/kg,five times per week)□low dose TC (50mg/kg□five times per week)and high dose TC (100mg/kg□five times per week), respectively. Tumor volume and body weight of mice were measured every three days. Compared with the vehicle group, Am-F4a and high dose TC significantly suppressed tumor growth (Fig. 5a,5b,5c)., no obvious mice body weight change was observed (Supplement Fig. 3a). Immunoblotting analysis of xenograft tumors demonstrated that Am-F4a significantly improved the level of cleaved-caspase-7, LC3-□and P62 protein, which indicated that Am-F4a might promote apoptosis and inhibit autophagy in the MGC803 xenograft tumors (Fig. 5d). Moreover, in a patient derived gastric cancer xenograft model (PDX), Am-F4a also effectively inhibited PDX tumor growth in a dose dependent manner. Interestingly, in line with the results *in vitro*, the combination of Am-F4a and 5-FU synergistically decreased PDX tumor growth in mice (Fig. 5e, 5f and supplement Fig. 3b), which indicated that Am-F4a might improve 5-FU treatment in GCa.

ATG4B inhibition inhibits GC tumor metastasis

Metastasis is a major cause of GCa-associated death, therefore we investigated whether ATG4B inhibitors could be used as anti-metastatic therapy. As shown in Figure, both ATG4B inhibitor Am-F4a and TC can significantly suppress migration and invasion of GC cells in vitro (Fig. 6a, 6b). Consistently, immunoblotting analysis demonstrated that ATG4B inhibition reduced the protein levels of key metastasis genes including snail and N-cadherin in cells (Fig. 6c, 6d). To assess the effects of Am-F4a on the gastric tumor metastasis *in vivo*, we established the orthotopic GCa metastasis models using MKN-45-luciferase cells. Tumor growth and metastasis were measured by bioluminescence (Fig. 6e). Compared to the vehicle group, both Am-F4a and 5-FU could effectively inhibit tumor growth and metastasis, and their combination showed strongest inhibition (Fig. 6e). Gastric cancer metastasis typically occurs in livers, peritoneum and lungs. Peritoneal metastasis index (PCI) is an effective indicator to evaluate peritoneal metastasis. After 18 days treatment, the mice was then euthanized and macroscopic appearance of GCa peritoneal metastases is shown as in Fig. 6f. Peritoneal metastatic nodules could be observed in all the vehicle treated mice, whereas only a few mice showed smaller metastatic nodules in the drug-treated mice. Consistently, Am-F4a and 5-FU effectively reduced mice PCI, and their combination resulted in lowest PCI (Fig. 6g). Moreover, Am-F4a also effectively inhibited the liver metastasis, suppressed GCa orthotopic tumor growth and sensitize tumor to 5-FU treatment

(Fig. 6h). Taken together, our data suggested that Am-F4a might be an effective agent for GC tumor metastasis therapy, especially combined with 5-FU treatment.

Discussion

In the past two decades, the prognosis for localized GCa has greatly improved, however, the outcomes of advanced disease remain poorly (42). Recently, promising progress has been made in targeted therapy for advanced GCa. Unfortunately, the options for targeted therapy and the number of patients benefited are limited. Discovery of new therapeutic targets and development of novel agents for advanced GC therapy are still urgently needed. Here, we demonstrated that ATG4B overexpression is significantly correlated with poor survival in patients with GC and is a critical dependency of GCa cell growth. Am-F4a, as a novel ATG4B inhibitor, potently inhibited GCa tumor growth and metastasis *in vitro* and *in vivo*.

ATG4B plays critical physiological roles in normal development and diseases via promoting autophagosome formation and autophagy process. In cancers, ATG4B has been identified as a potential therapeutic target in a number of cancers, including colon, glioblastoma, osteosarcoma. Our study here advanced our understanding of the functions of ATG4B in GCa. Analysis of patient samples showed that ATG4B is overexpressed in GCa tumors, and its high expression correlated with patients' poor survival. Silencing ATG4B with specific siRNAs significantly inhibited GCa cell autophagy, survival and promoted their apoptosis. Notably, knockdown of ATG4B potently suppressed tumorigenesis and tumor growth in mice GCa xenograft models. Therefore, ATG4B is essential for GCa cell survival and tumor growth.

Recently, several ATG4B inhibitors were discovered and used to explore the physiological functions of ATG4B in cancers. In line with the effect of ATG4B silencing in cancer cells, most of ATG4B inhibitors exerted anti-cancer activity via suppressing autophagy process. However, the efficacy and diversity of current ATG4B inhibitors are limited. A potent and selective ATG4B inhibitor is still needed to explore the therapeutic potentials of ATG4B inhibition. Here, we discovered a novel ATG4B inhibitor, Am-F4a, from a natural product library. FRET assay and SPR analysis demonstrated that Am-F4a selectively bound to ATG4B protein and potently inhibited ATG4B activity. Molecular docking study indicated that Am-F4a could form several H-bonds with ATG4B in binding pocket site 5 (Fig. 2f and 2g), and especially the H-bond between guanidine group of Am-F4a and residue Asn261 in the regulatory loop (residues 259 to 262) of the entrance of catalytic site makes Am-F4a a potent inhibitor for ATG4B from the atomic level perspective. In cancer cells, Am-F4a effectively inhibited autophagic flux and accumulated lapidated LC3 in autolysosomes. These data suggested that Am-F4a might be an excellent lead compound to uncover the pharmacological roles of ATG4B in cancers.

Notably, our data revealed that Am-F4a significantly inhibited GCa cell growth and triggered their apoptosis via suppressing ATG4B activity. Moreover, Am-F4a potently inhibited tumor growth in both cell line-derived and patient-derived GCa xenograft models without obvious toxicity. Chemotherapy resistance and metastasis are the main obstacles for advanced GCa therapy. Several studies indicated that ATG4B inhibition might be helpful to overcome drug resistance, however, the pharmacological roles of ATG4B in

cancer metastasis remained unknown. We found that genetic and pharmacologic inhibition of ATG4B significantly suppressed GCa cell migration and invasion *in vitro*. Employing orthotopic GCa metastasis xenograft models, we demonstrated herein that Am-F4a could markedly block liver and peritoneal metastasis, and sensitized tumors to 5-fu treatment. 5-fu chemotherapy is the first choice for advanced GCa therapy, but its effectiveness is limited by drug resistance. Therefore, this study suggested that ATG4B inhibition might have broad clinical utilities in GCa. Our data showed that the effect of ATG4B inhibition on GCa cells might be through suppressing autophagy process. Genetic and pharmacological inhibition of ATG4B significantly inhibited autophagic flux and accumulated lapidated LC3 in autolysosomes both in vitro and in vivo. However, the overall impact of ATG4B inhibition on tumor growth is unlikely limited to suppressing autophagy. Previous study showed that ATG4B knockdown increased CCND1 expression and resulted in colorectal cancer cell growth arrest independent of autophagy,(43) our study also showed that ATG4B inhibition increased CCND1 expression in GCa cells (Supplement Fig. 5a). Therefore, ATG4B inhibition blocks GCa tumor growth and metastasis, possibly through inhibiting multiple pathways, including autophagy.

Conclusion

In summary, we demonstrated here that ATG4B might be a potential therapeutic target for advanced GCa and identified a natural product Am-F4a as a novel ATG4B inhibitor. Am-F4a significantly inhibited GCa cell survival and tumor growth via suppressing ATG4B activity and downstream processes. Furthermore, in orthotopic GCa metastasis xenograft models, we found that Am-F4a could effectively block GCa liver and peritoneal metastasis, and sensitized tumors to 5-FU treatment. These data collectively suggested that ATG4B inhibition might have a broad clinical utility in GCa, and Am-F4a might be is an efficacious antitumor therapeutic agent.

Abbreviations

GCa: Gastric cancer; Am-F4a: Azalomycin F4a□ ATG4: Autophagy-related gene 4; Rap: Rapamycin; Baf□ BafilomycinA1; TC: Tioconazole; CQ: chloroquine; AO: Acridine Orange; LTR: Lyso-Tracker Red; SPR: surface plasmon resonance; FRET: Förster resonance energy transfer; TEM: Transmission electron microscopy; PDO: Patient-derived organoid ; PDX: patient-derived xenograft; PCI: Peritoneal metastasis index.

Declarations

Ethics approval and consent to participate

All clinical studies were approved by the Clinical Research Ethics Committee of Sun Yat-sen University, and were performed in accordance with approved guidelines (Helsinki Declaration of 2013). All animal experiments were conducted in accordance with the “Guiding Principles in the Care and Use of Animals” (China) and were approved by the Animal Ethics Committee at Sun Yat-sen University.

Consent for publication

All authors have provided their consent for publication.

Availability of data and materials

The data sets used and analyzed during the current study are available from the corresponding author on reasonable request.

Completing Interests

The authors declare no competing financial interests.

Funding

This research was supported by the National Natural Science Foundation of China (No.81872891, 81572925, 81903081 and 41776169),the Guangdong Natural Science Funds for Distinguished Young Scholar (No. 2019B151502016), Guangdong Natural Science Funds (No. 2021A1515012029), Guangzhou Science and Technology Basic Research Program (No. 202002020082),Local Innovative and Research Teams Project of Guangdong Pearl River Talents Program (2017BT01Y093), National Major Special Projects for the Creation and Manufacture of New Drugs (2019ZX09301104), National Engineering and Technology Research Center for New drug Druggability Evaluation (Seed Program of Guangdong Province, 2017B090903004),the Fundamental Research Funds for the Central Universities (No. 19ykzd23), the Finance Science and Technology Project of Hainan Province (ZDKJ202018).

Authors' contributions

L Z, BY, and ZHZ designed the research, performed experiments, analyzed data, and wrote the manuscript. L Z, BY, and ZHZ contributed equally to this work, XJW and PQL helped perform the experiments and provided the funding. YFG, WFH, QQW, GDC, and FX helped perform the experiments. SNZ, SM helped with data analysis and interpretation. YCN, JPL, ML, WBD, and YHL reviewed the manuscript. JJW, FHH, and JFW supervised the experiments and provided the funding. All authors read and approved the final manuscript.

Acknowledgements

We thank Hong-Wu Chen (UC Davis) for his thoughtful advice regarding the study design, experiments, and language editing.

Authors' information

[a] Department of Gastrointestinal Surgery, Sun Yat-sen Memorial Hospital, Sun Yat-sen University, Guangzhou, Guangdong 510120, China;

[b] Department of Pharmaceutical Sciences (Shenzhen), Sun Yat-Sen University, Guangzhou, Guangdong 510006, China;

[c] Hepatopancreatobiliary Center, Beijing Tsinghua Changgung Hospital, Tsinghua University, No.168, Litang Road, Changping District, Beijing 102218, China.;

[d] School of Pharmaceutical Sciences, Sun Yat-sen University, Guangzhou, Guangdong, 510006, China

[e] Guangdong Provincial Key Laboratory of New Drug Design and Evaluation, National-Local Joint Engineering Laboratory of Druggability and New Drugs Evaluation, Sun Yat-sen University, Guangzhou, Guangdong, 510006, China.

[f] CAS Key Laboratory of Tropical Marine Bio-resources and Ecology/Guangdong Key Laboratory of Marine Materia Medica, South China Sea Institute of Oceanology, Chinese Academy of Sciences, Guangzhou 510301, China;

References

1. Sung H, Ferlay J, Siegel RL, Laversanne M, Soerjomataram I, Jemal A, et al. Global cancer statistics 2020: GLOBOCAN estimates of incidence and mortality worldwide for 36 cancers in 185 countries. CA Cancer J Clin. 2021.
2. Park S, Nam CM, Kim SG, Mun JE, Rha SY, Chung HC. Comparative efficacy and tolerability of third-line treatments for advanced gastric cancer: A systematic review with Bayesian network meta-analysis. Eur J Cancer. 2021;144:49–60.
3. Jin X, Zhu Z, Shi Y. Metastasis mechanism and gene/protein expression in gastric cancer with distant organs metastasis. Bull Cancer. 2014.
4. Digklia A, Wagner AD. Advanced gastric cancer: Current treatment landscape and future perspectives. World J Gastroenterol. 2016;22(8):2403–14.
5. Tan Z. Recent Advances in the Surgical Treatment of Advanced Gastric Cancer: A Review. Med Sci Monit. 2019;25:3537–41.
6. Smyth EC, Verheij M, Allum W, Cunningham D, Cervantes A, Arnold D, et al. Gastric cancer: ESMO Clinical Practice Guidelines for diagnosis, treatment and follow-up. Ann Oncol. 2016;27(suppl 5):v38–49.
7. Smyth EC, Nilsson M, Grabsch HI, van Grieken NC, Lordick F. Gastric cancer. Lancet. 2020;396(10251):635–48.
8. Goetze OT, Al-Batran SE, Chevallay M, Monig SP. Multimodal treatment in locally advanced gastric cancer. Updates Surg. 2018;70(2):173–9.
9. National Health Commission Of The People's Republic Of C. Chinese guidelines for diagnosis and treatment of gastric cancer 2018 (English version). Chin J Cancer Res. 2019;31(5):707–37.

10. Japanese Gastric Cancer A. Japanese gastric cancer treatment guidelines 2018 (5th edition). Gastric Cancer. 2020.
11. Kotani D, Shitara K. Trastuzumab deruxtecan for the treatment of patients with HER2-positive gastric cancer. Ther Adv Med Oncol. 2021;13:1758835920986518.
12. Chau I, Penel N, Soriano AO, Arkenau HT, Cultrera J, Santana-Davila R, et al. Ramucirumab in Combination with Pembrolizumab in Treatment-Naive Advanced Gastric or GEJ Adenocarcinoma: Safety and Antitumor Activity from the Phase 1a/b JVDF Trial. Cancers (Basel). 2020;12(10).
13. Fu Y, Huang Z, Hong L, Lu JH, Feng D, Yin XM, et al. Targeting ATG4 in Cancer Therapy. Cancers (Basel). 2019;11(5).
14. Fu Y, Hong L, Xu J, Zhong G, Gu Q, Gu Q, et al. Discovery of a small molecule targeting autophagy via ATG4B inhibition and cell death of colorectal cancer cells in vitro and in vivo. Autophagy. 2019;15(2):295–311.
15. Lystad AH, Simonsen A. Mechanisms and Pathophysiological Roles of the ATG8 Conjugation Machinery. Cells. 2019;8(9).
16. Li M, Hou Y, Wang J, Chen X, Shao ZM, Yin XM. Kinetics comparisons of mammalian Atg4 homologues indicate selective preferences toward diverse Atg8 substrates. J Biol Chem. 2011;286(9):7327–38.
17. Agrotis A, Pengo N, Burden JJ, Ketteler R. Redundancy of human ATG4 protease isoforms in autophagy and LC3/GABARAP processing revealed in cells. Autophagy. 2019;15(6):976–97.
18. Cabrera S, Fernandez AF, Marino G, Aguirre A, Suarez MF, Espanol Y, et al. ATG4B/autophagin-1 regulates intestinal homeostasis and protects mice from experimental colitis. Autophagy. 2013;9(8):1188–200.
19. Cabrera S, Maciel M, Herrera I, Nava T, Vergara F, Gaxiola M, et al. Essential role for the ATG4B protease and autophagy in bleomycin-induced pulmonary fibrosis. Autophagy. 2015;11(4):670–84.
20. Agrotis A, Ketteler R. On ATG4B as Drug Target for Treatment of Solid Tumours-The Knowns and the Unknowns. Cells. 2020;9(1).
21. Huang T, Kim CK, Alvarez AA, Pangeni RP, Wan X, Song X, et al. MST4 Phosphorylation of ATG4B Regulates Autophagic Activity, Tumorigenicity, and Radioresistance in Glioblastoma. Cancer Cell. 2017;32(6):840–55. e8.
22. Wu S, Su J, Qian H, Guo T. SLC27A4 regulate ATG4B activity and control reactions to chemotherapeutics-induced autophagy in human lung cancer cells. Tumour Biol. 2016;37(5):6943–52.
23. Li Y, Li C, Li D, Yang L, Jin J, Zhang B. lncRNA KCNQ1OT1 enhances the chemoresistance of oxaliplatin in colon cancer by targeting the miR-34a/ATG4B pathway. Onco Targets Ther. 2019;12:2649–60.
24. Rothe K, Lin H, Lin KB, Leung A, Wang HM, Malekesmaeili M, et al. The core autophagy protein ATG4B is a potential biomarker and therapeutic target in CML stem/progenitor cells. Blood. 2014;123(23):3622–34.

25. Liu PF, Tsai KL, Hsu CJ, Tsai WL, Cheng JS, Chang HW, et al. Drug Repurposing Screening Identifies Tioconazole as an ATG4 Inhibitor that Suppresses Autophagy and Sensitizes Cancer Cells to Chemotherapy. Theranostics. 2018;8(3):830–45.
26. Akin D, Wang SK, Habibzadegah-Tari P, Law B, Ostrov D, Li M, et al. A novel ATG4B antagonist inhibits autophagy and has a negative impact on osteosarcoma tumors. Autophagy. 2014;10(11):2021–35.
27. Bishayee A, Sethi G. Bioactive natural products in cancer prevention and therapy: Progress and promise. Semin Cancer Biol. 2016;40–41:1–3.
28. Newman DJ, Cragg GM. Natural Products as Sources of New Drugs over the Nearly Four Decades from 01/1981 to 09/2019. J Nat Prod. 2020;83(3):770–803.
29. Carroll AR, Copp BR, Davis RA, Keyzers RA, Prinsep MR. Marine natural products. Nat Prod Rep. 2021.
30. Milunovic V, Misura Jakobac K, Kursar M, Mandac Rogulj I, Ostojic Kolonic S. FDA's and EMA's approval of brentuximab vedotin for advanced Hodgkin lymphoma: Another player in the town? Eur J Haematol. 2019;103(3):145–51.
31. Koyama N, Taniguchi S, Kodama K, Tohyama O, Hasegawa H, Semba T. Clinical benefit of eribulin (Halaven((R))) in the treatment of advanced soft tissue sarcoma patients and the novel anti-tumor mechanisms. Nihon Yakurigaku Zasshi. 2016;148(6):329–33.
32. Souid S, Aissaoui D, Srairi-Abid N, Essafi-Benkhadir K. Trabectedin (Yondelis(R)) as a Therapeutic Option in Gynecological Cancers: A Focus on its Mechanisms of Action, Clinical Activity and Genomic Predictors of Drug Response. Curr Drug Targets. 2020;21(10):996–1007.
33. Walter RB, Appelbaum FR, Estey EH. Optimal dosing of cytarabine in induction and post-remission therapy of acute myeloid leukemia. Leukemia. 2021;35(2):295–8.
34. Wang J, Cong Z, Huang X, Hou C, Chen W, Tu Z, et al. Soliseptide A, A Cyclic Hexapeptide Possessing Piperazic Acid Groups from Streptomyces solisilvae HNM30702. Org Lett. 2018;20(5):1371–4.
35. Zheng J, Wang J, Wang Q, Zou H, Wang H, Zhang Z, et al. Targeting castration-resistant prostate cancer with a novel RORgamma antagonist elaiophylin. Acta Pharm Sin B. 2020;10(12):2313–22.
36. Zhang Y, Wu X, Xue X, Li C, Wang J, Wang R, et al. Discovery and Characterization of XY101, a Potent, Selective, and Orally Bioavailable RORgamma Inverse Agonist for Treatment of Castration-Resistant Prostate Cancer. J Med Chem. 2019;62(9):4716–30.
37. Fu Y, Gu Q, Luo L, Xu J, Luo Y, Xia F, et al. New Anti-Cancer Strategy to Suppress Colorectal Cancer Growth Through Inhibition of ATG4B and Lysosome Function. Cancers (Basel). 2020;12(6).
38. Kimura S, Noda T, Yoshimori T. Dissection of the autophagosome maturation process by a novel reporter protein, tandem fluorescent-tagged LC3. Autophagy. 2007;3(5):452–60.
39. Chu J, Fu Y, Xu J, Zheng X, Gu Q, Luo X, et al. ATG4B inhibitor FMK-9a induces autophagy independent on its enzyme inhibition. Arch Biochem Biophys. 2018;644:29–36.
40. Klionsky DJ, Abdelmohsen K, Abe A, Abedin MJ, Abeliovich H, Acevedo Arozena A, et al. Guidelines for the use and interpretation of assays for monitoring autophagy (3rd edition). Autophagy.

2016;12(1):1-222.
41. Hou X, Jiang J, Tian Z, Wei L. Autophagy and Tumour Chemotherapy. Adv Exp Med Biol. 2020;1207:351–74.
42. Kawazoe A, Shitara K, Boku N, Yoshikawa T, Terashima M. Current status of immunotherapy for advanced gastric cancer. Jpn J Clin Oncol. 2021;51(1):20–7.
43. Liu PF, Leung CM, Chang YH, Cheng JS, Chen JJ, Weng CJ, et al. ATG4B promotes colorectal cancer growth independent of autophagic flux. Autophagy. 2014;10(8):1454–65.

Figures

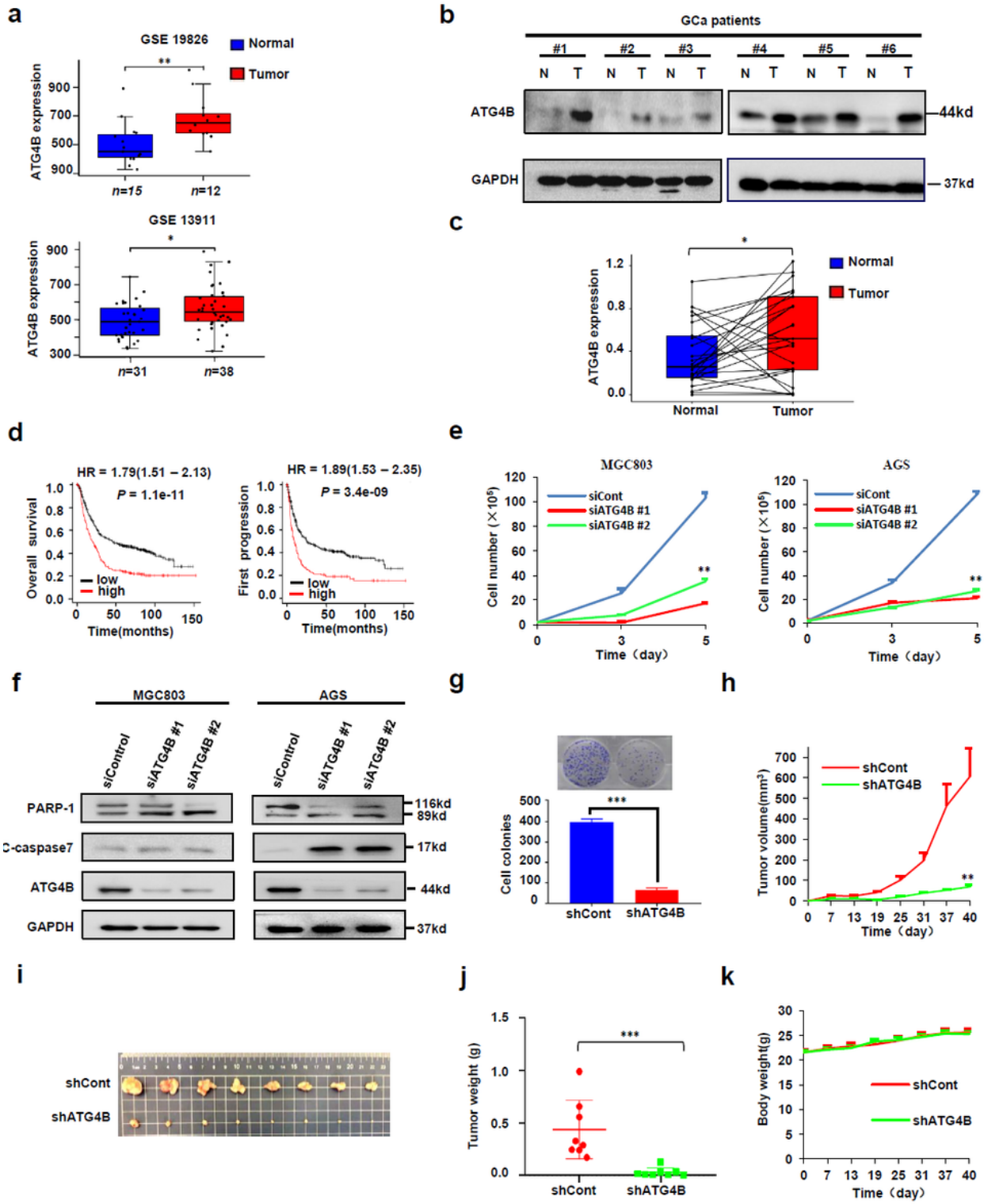

Figure 1

ATG4B is highly over expressed in GCa clinical tumors and is required for GCa cell growth (a) ATG4B transcript levels from two GEO datasets were queried for association with disease status（normal and tumor). P value were calculated by using two-tailed Student's t-test. * $p < 0.05$, ** $p < 0.001$. (b and c) ATG4B protein levels were analyzed by immunoblotting analysis of in tissues (tumor and adjacent normal tissues) and representative images were shown. The data were statistically analyzed as in (a). (d)

Kaplan-Meier overall survival and relapse curve analysis of GCa patients, stratified by ATG4B expression (data were obtained from: https://kmplot.com/analysis/). (e) MGC803 and AGS cells were transfected with ATG4B or control siRNA. After indicated time points, viable cells were counted. Data shown are mean ± SD. Student's t-test. **p < 0.01, n = 3. (f) Immunobloting analysis of indicated protein in MGC803 and AGS cells transfected with ATG4B or control siRNA and incubated for two days. Representative blot, n = 3. (g) Colony formation of MGC803 cells infected with control or ATG4B shRNA lentiviruses. Representative images were shown, and colonies were counted. n = 3. (h - k) MGC803 cells infected with control or shATG4B lentiviruses expression shRNA were injected into the dorsal flank of mice. Tumor growth and mice body weight was monitored. Representative tumor image and tumor weight at the end time point was captured. Mean tumor volume ± S.E.M (h), mean tumor weight ± S.E.M (j) and mean mice body weight ± S.E.M (k) were shown. Significance was calculated using two-tailed Student's t-test, **p < 0.01, ***P < 0.001.

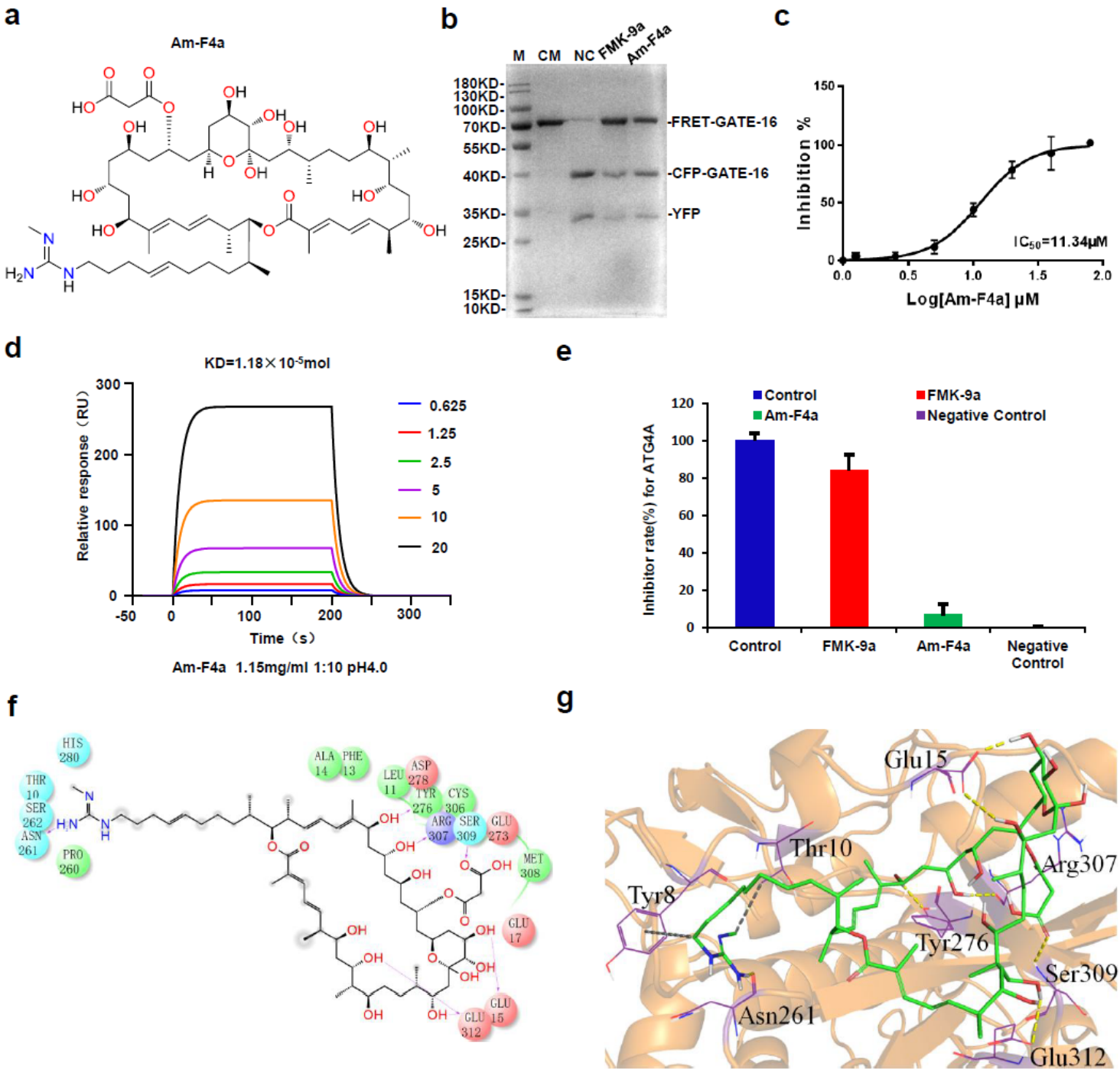

Figure 2

Identification of Am-F4a as a novel ATG4B inhibitor (a) Chemical structure of Am-F4a. (b) ATG4B (0.75 μg/ml) was incubated with or without Am-F4a (10 μM) at 37°C for 30 min, FRET-GATE-16 was then added and incubated at 37°C for another 30 min. The inhibitory effect of Am-F4a was detected by SDS-PAGE according to the cleavage of FRET substrates. FMK-9a was used as a positive control. (c) The inhibitory effect and IC50 of Am-F4a on ATG4B activity was obtained from FRET assay. (d) Surface plasmon resonance (SPR) analysis of binding affinity of Am-F4a to ATG4B. The Kd value was calculated based on the fitted curves. (e) Am-F4a on ATG4A activity, the inhibitory effect of Am-F4a was detected by FREAT. (f

and g) The predicted 2D and 3D binding mode of Am-F4a with ATG4B by molecular docking. In 3D mode, the protein and ligand Am-F4a are shown by cartoon and stick respectively, the highlighted interacting residues are shown by lines, the hydrogen bonds are labeled by yellow dashed lines, and the hydrophobic interaction are labeled by gray dashed lines .

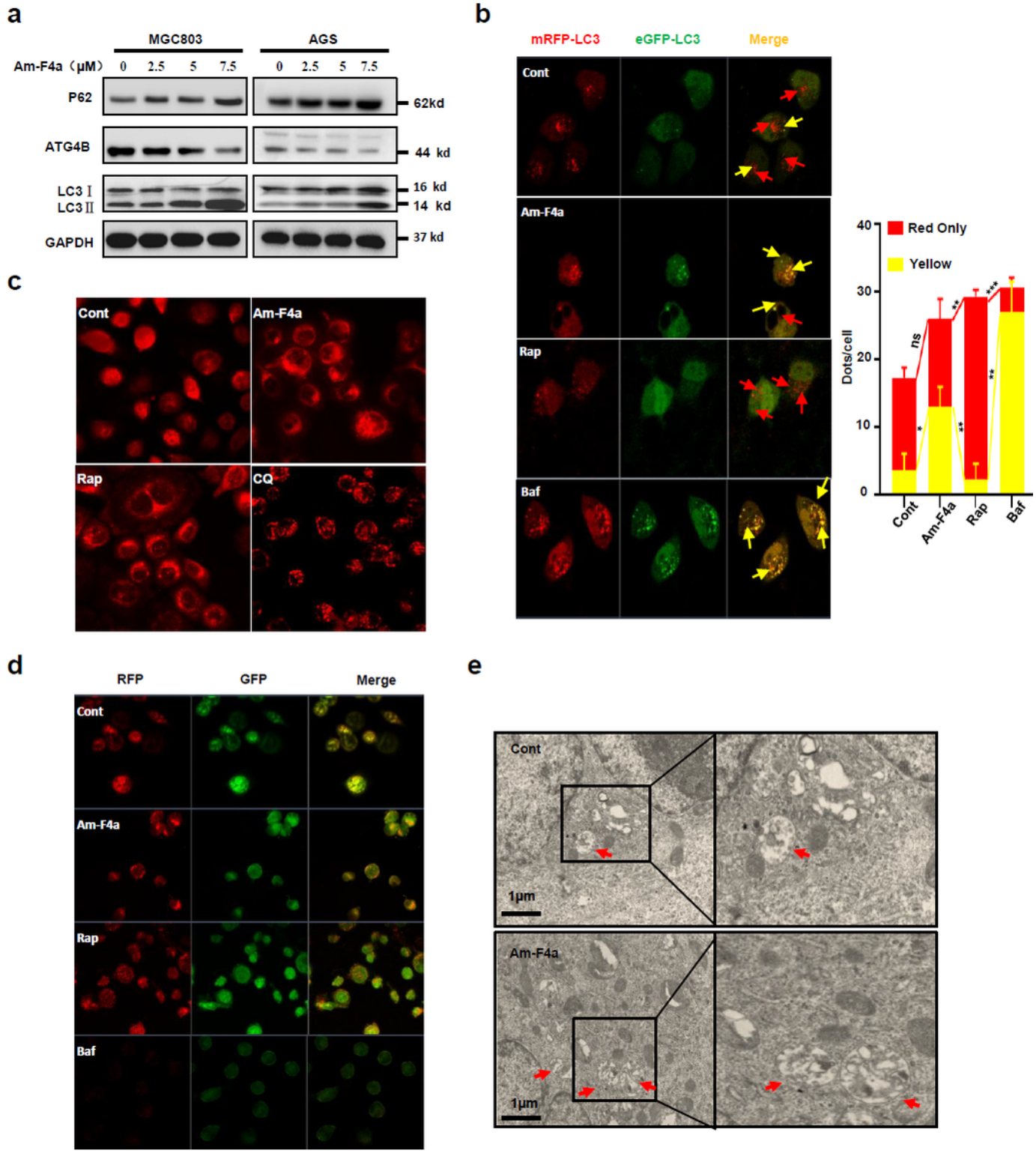

Figure 3

Am-F4a suppresses autophagy flux and accumulates autolysosomes with more lipidated LC3 (a) Immunobloting analysis of indicated protein in MGC803 and AGS cells treated with Am-F4a for 48 hours. Representative blots, n = 3. (b) MGC803 cells expressing GFP-RFP-LC3 were treated with Am-F4a (10 μM) Rap (1 μM) and Baf 0.5μM for 6 hours. The colocalization of GFP and RFP puncta was examined and quantified. Red arrows indicate GFP- or LC3-positive structure, yellow arrows indicate the colocalization of GFP and RFP. Fluorescence images of live cells were recorded with fixation. Data are shown as mean ± SD, n = 3, Student's t test, *p<0.05, **p<0.01, ***p < 0.001. (c and d) LTR (red), AO (orange) can indicate normal autolysosome structures of cells. AGS cells were treated with Am-F4a (10 μM),Rap (1 μM) ,Baf 0.5μM or Chloroquine CQ 40μM for 4 hours, followed by staining with Lyso-Tracker Red (LTR, 50 ng/ml) or Acridine Orange (AO, 0.5μg/ml) for 30 min. Fluorescence images of live cells were recorded without fixation. (e) Representative images of transmission electron microscopy (TEM) exhibit ultrastructure of MGC803cells treated with or without Am-F4a (10 μM) for 6 hours. Red arrows indicate normal autophagosome structures.

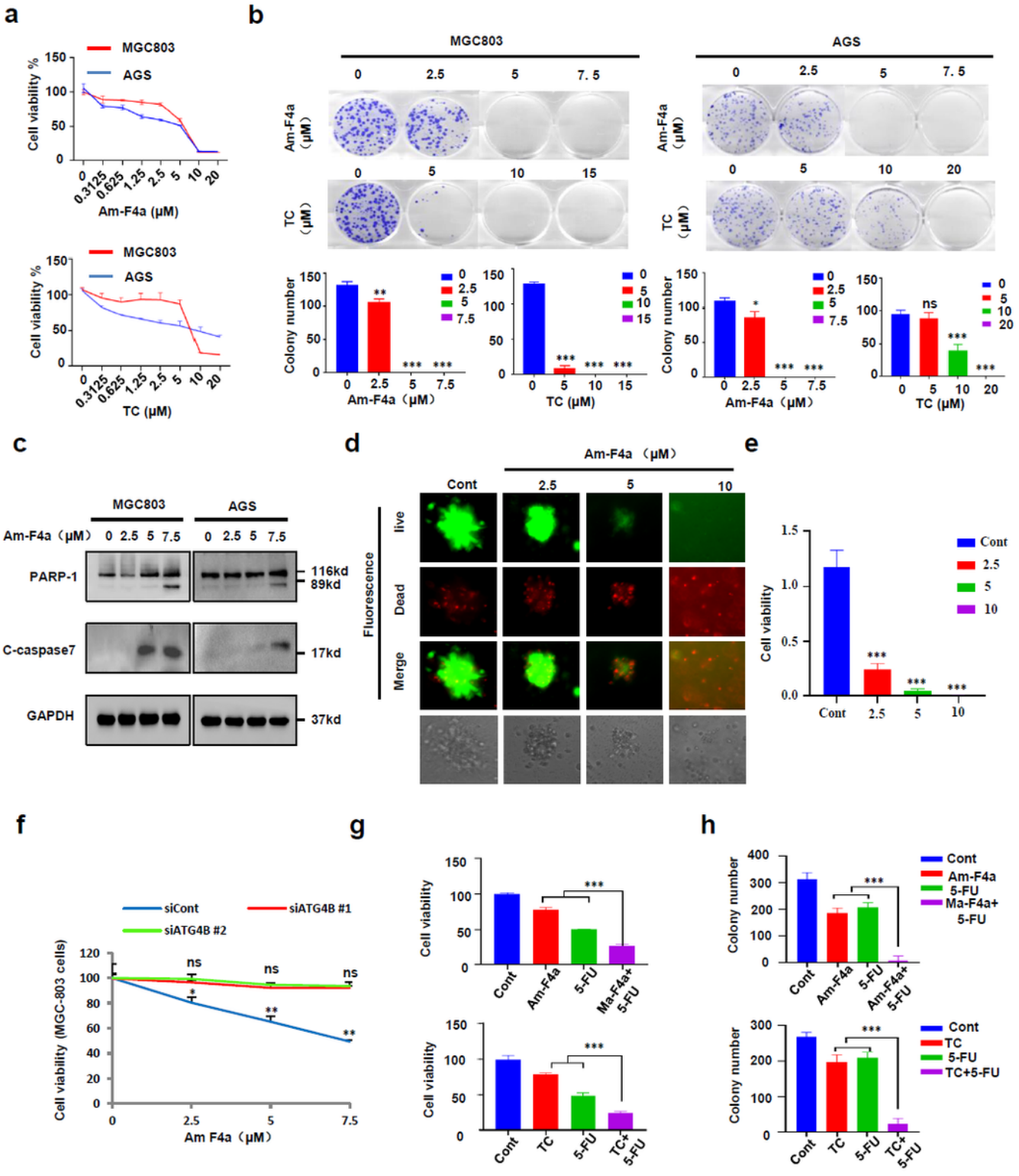

Figure 4

Am-F4a inhibits GCa cell growth via inhibition of ATG4B and improve anti-GCa efficacy of 5-FU (a) Cell viability was evaluated by CCK-8 assay of MGC803 and AGS cells treated with Am-F4a and Tioconazole (TC). (b) Colony formation of MGC803 and AGS cells treated with Am-F4a at indicated concentration. Representative images were shown, and colonies were counted. (c) Immunoblotting analysis of cleaved PARP-1 and caspase 7 in MGC803 and AGS cells treated with Am-F4a at indicated concentration.

Representative blot was shown. (d and e) PDX-derived organoids were treated with DMSO or indicated concentrations of Am-F4a for 4 days. Representative images were taken under a fluorescence microscope or a standard light microscope (d), scale bar,100 μm. Cell viability in organoids was measured with Cell Titer-Glo (e). (f) MGC803 cells were transfected with ATG4B or control siRNA for 48 hours and then treated with Am-F4a at for another 24 hours. Viable cells were collected and counted. (g) MGC803 cells were treated with Am-F4a (4μM) or TC（5μM）alone, or in combination with 5-FU（2μM）for 48 hours. Viable cells were collected and counted. (h) MGC803 cells were treated with Am-F4a (4μM) or TC（5μM）alone, or in combination with 5-FU（2μM）for 48 hours. Colonies were stained and counted. All data shown above are mean ± SD, n = 3, Student's t test, *p<0.05, **p<0.01, ***p < 0.001.

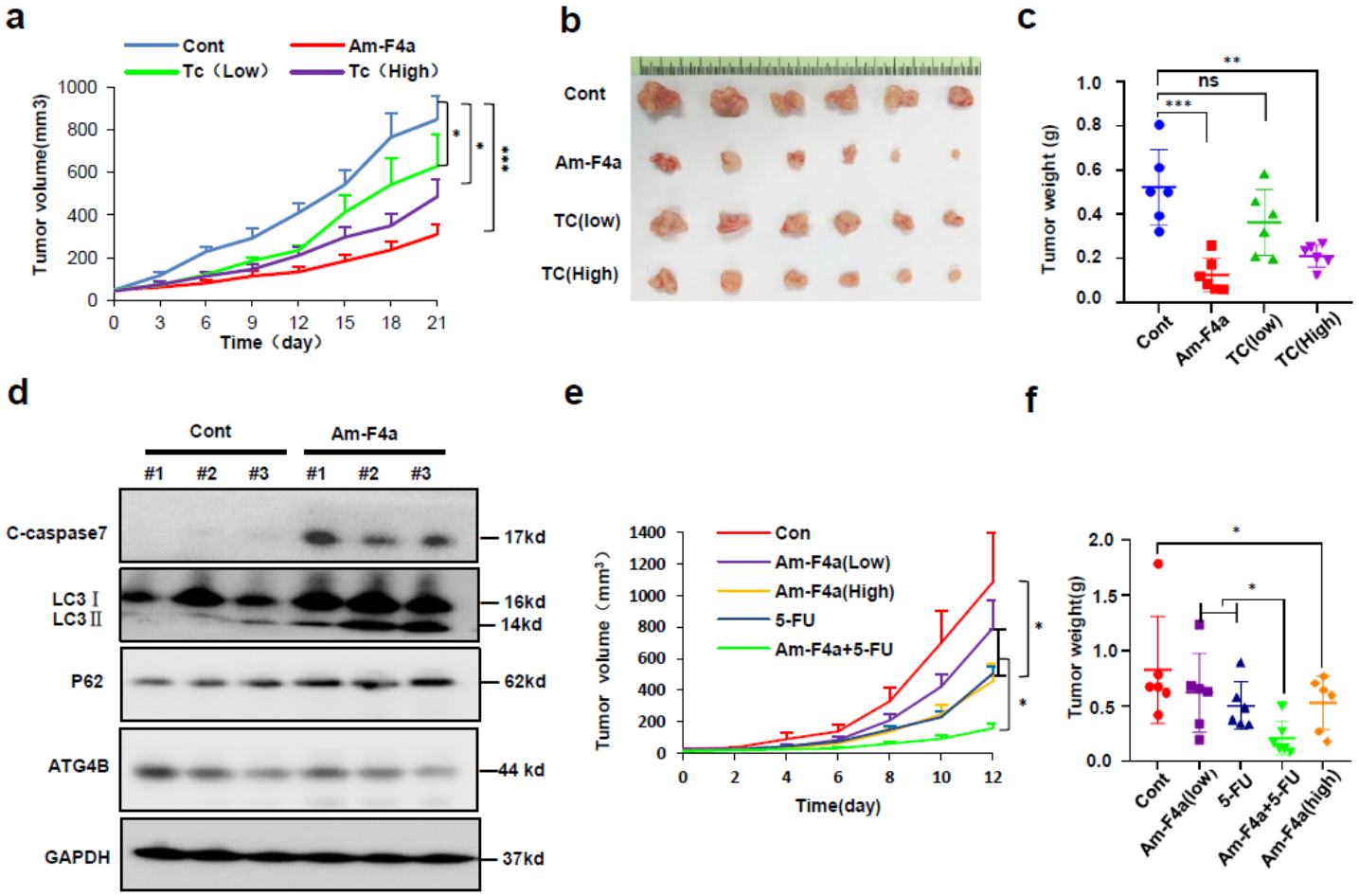

Figure 5

Pharmacological inhibition of ATG4B with Am-F4a inhibits GCa tumor growth and improves 5-FU treatment in vivo (a - c) Effects of the indicated treatments (Am-F4a 5 mg/kg, TC low 50mg/kg, TC high 100mg/kg, or vehicle, i.p., 5 times per week) on the growth of MGC803 cell-based xenografts. Representative tumor image and tumor weight at the end time point was captured. Mean tumor volume ± S.E.M (a) and mean tumor weight ± S.E.M (c) was shown. (d) Immunoblotting analysis of indicated proteins in MGC803 xenograft tumors after 21 days of treatment with vehicle or Am-F4a, as in (a), representative image was shown. (e and f) Effects of the indicated treatments (Am-F4a low 2.5mg/kg、Am-F4a high 5mg/kg, 5-FU 20mg/kg, Am-F4a low 2.5mg/kg and 5-FU 20mg/kg, or vehicle, i.p., 5 times

per week) on the growth of PDX xenografts. Mean tumor volume ± S.E.M (e) and mean tumor weight ± S.E.M (f) was shown. All Data shown above was calculated using two-tailed Student's t-test, n = 6 mice per group, *P < 0.05, **P < 0.01, ***P < 0.001.

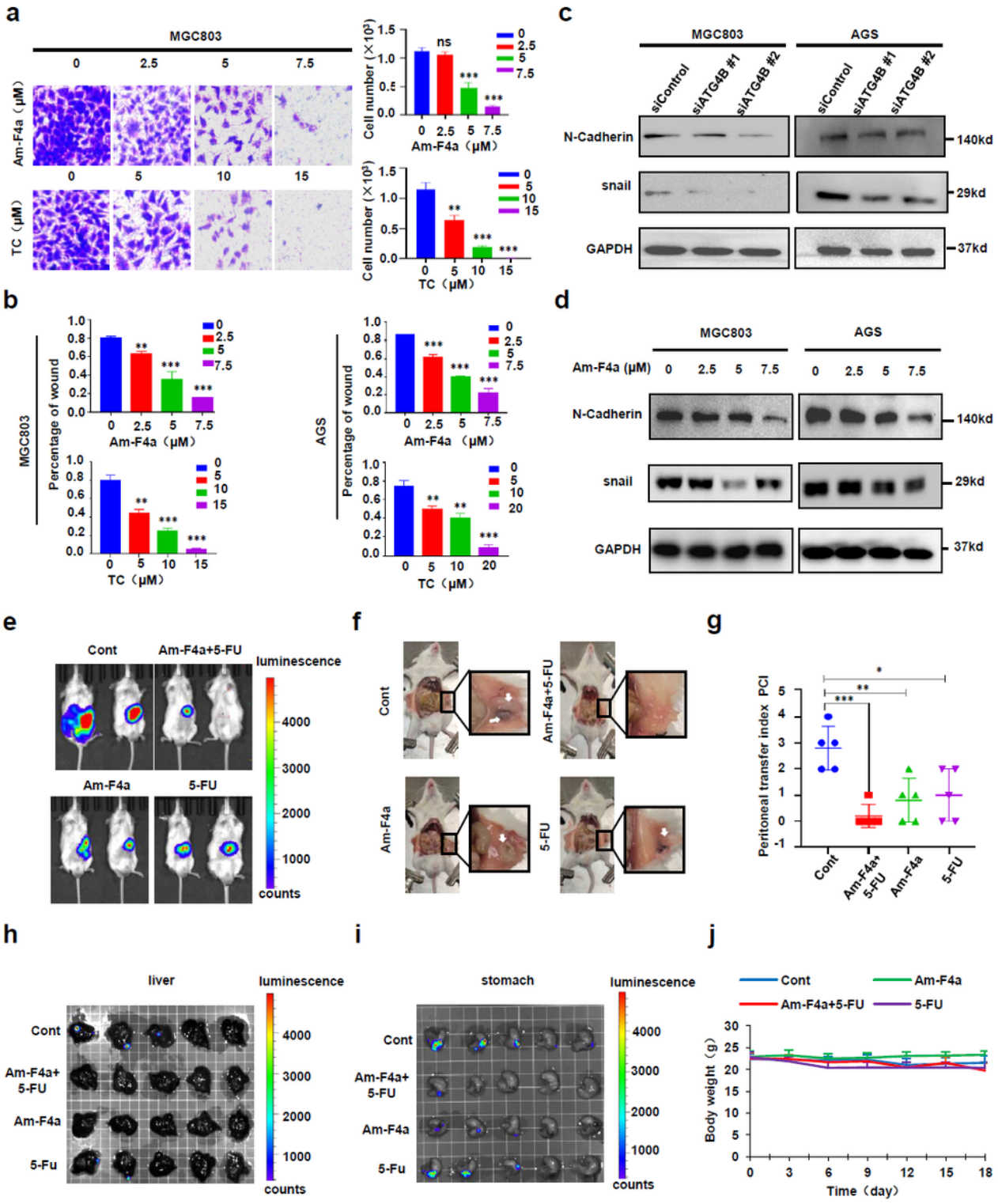

Figure 6

ATG4B inhibition inhibits GC tumor metastasis (a) The invasion ability of MGC803 cells treated with Am-F4a, TC or vehicle at indicated concentration were evaluated by transwell assay. (b) The migration of GCa

cells were determined using would healing assay. (c) Immunobloting analysis of indicated proteins in MGC803 and AGS cells transfected with ATG4B or control siRNA and incubated for 48 hours. (d) Immunoblotting analysis of indicated proteins in MGC803 and AGS cells treated with Am-F4a or vehicle for 48 hours. (e) MKN-45 cells stable expressing mCherry-Luciferase were injected into the stomach wall of NCG mice, and randomly divided into four groups as indicated. Tumors growth in the stomach wall and metastases to the peritoneal cavity or other organs were monitored by bioluminescence at 14th days. (f and g) Representative image of the peritoneal metastasis (white arrows) of MKN-45 cells in mice at the end of study (f). The peritoneal nodules were evaluated by peritoneal metastasis index (PCI) (g). (h and i) Metastasis on the liver and stomach were monitored by bioluminescence at the end of study. (j) The body weight of the mice in all groups have no obviously change. All Data shown above was calculated using two-tailed Student's t-test, results of animal experiments were shown as mean± S.E.M, n = 5mice per group. Cell culture experiments were repeated at least three times and shown as mean ± SD. *P < 0.05, **P < 0.01, ***P < 0.001.

Supplementary Files

This is a list of supplementary files associated with this preprint. Click to download.

- supplement.docx